

Published in final edited form as:

*Anal Chem.* 2011 June 15; 83(12): 4962–4969. doi:10.1021/ac200693h.

## Brominated Tyrosine and Polyelectrolyte Multilayer Analysis by Laser Desorption VUV Postionization and Secondary Ion Mass Spectrometry

M.T. Melvin Blaze<sup>1</sup>, Lynelle K. Takahashi<sup>2,3</sup>, Jia Zhou<sup>3,J</sup>, Musahid Ahmed<sup>3</sup>, Gerald L. Gasper<sup>1</sup>, F. Douglas Pleticha<sup>1</sup>, and Luke Hanley<sup>1,\*</sup>

<sup>1</sup> Department of Chemistry, University of Illinois at Chicago, Chicago, IL 60607

<sup>2</sup> Department of Chemistry, University of California, Berkeley, Berkeley, CA 94720

<sup>3</sup> Chemical Sciences Division, Lawrence Berkeley National Laboratory, Berkeley, CA 94720

### Abstract

The small molecular analyte 3,5-dibromotyrosine (Br<sub>2</sub>Y) and chitosan-alginate polyelectrolyte multilayers (PEM) with and without adsorbed Br<sub>2</sub>Y were analyzed by laser desorption postionization mass spectrometry (LDPI-MS). LDPI-MS using 7.87 eV laser and tunable 8 – 12.5 eV synchrotron vacuum ultraviolet (VUV) radiation found that desorption of clusters from Br<sub>2</sub>Y films allowed detection by ≤8 eV single photon ionization. Thermal desorption and electronic structure calculations determined the ionization energy of Br<sub>2</sub>Y to be ~8.3±0.1 eV and further indicated that the lower ionization energies of clusters permitted their detection at ≤8 eV photon energies. However, single photon ionization could only detect Br<sub>2</sub>Y adsorbed within PEMs when using either higher photon energies or matrix addition to the sample. All samples were also analyzed by 25 keV Bi<sub>3</sub><sup>+</sup> secondary ion mass spectrometry (SIMS), with the negative ion spectra showing strong parent ion signal which complemented that observed by LDPI-MS. However, the negative ion SIMS appeared strongly dependent on the high electron affinity of this specific analyte and the analyte's condensed phase environment.

### I. INTRODUCTION

Bacterial biofilms consist of colonies of microbial cells embedded in an extracellular polysaccharide matrix which are often attached to solid surfaces.<sup>1</sup> They are responsible for a large number of medical infections and play a role in environmental and industrial processes. The structure and composition of these microbial biofilm communities depend on the properties of their anchoring surface since the metabolism of individual microbes is affected by their environment. Given that even a single species biofilm is composed of microbial cells in different metabolic states, imaging of intact biofilms will provide chemical information not available to studies of homogenized microbial extracts.

Mass spectrometric (MS) imaging can probe chemical distributions of metabolites and signaling molecules within intact bacterial biofilms to help elucidate the role of metabolic state and environment. Secondary ion mass spectrometry (SIMS) is one MS imaging method that has been applied to bacterial biofilms and other intact biological tissue.<sup>2–5</sup>

\*Corresponding author, L.Hanley@uic.edu.

<sup>J</sup>Current address: Chemistry Department, Brookhaven National Laboratory, Upton, NY

The authors are developing two other methods for MS imaging analyses of bacterial biofilms and other samples: laser desorption postionization mass spectrometry (LDPI-MS)<sup>6,7</sup> and secondary neutral mass spectrometry (SNMS).<sup>8,9</sup> Both methods rely upon vacuum ultraviolet (VUV) single photon ionization (SPI) of laser desorbed or ion sputtered neutrals.<sup>10</sup> Recent LDPI-MS work has focused on SPI with 7.87 eV VUV radiation because it is available from a convenient laboratory source – the molecular fluorine laser which emits at 157.6 nm. However, its 7.87 eV photon energy is below the ionization energy of many analytes, limiting the potential targets that it can ionize. 10.5 eV VUV radiation from the 118 nm ninth harmonic of the Nd:YAG laser has historically been the most popular VUV source for SPI because of its ability to ionize a much larger class of molecular analytes while avoiding detection of water, carbon dioxide and other abundant species usually of little interest to MS imaging.<sup>10</sup> However, the 10.5 eV source suffers from a relatively low, ~nJ energy per pulse which limits sensitivity and precludes its use in commercial instruments.

The question arises as to what VUV photon energies are most effective for postionization. Photon energies that are slightly above the ionization threshold of a molecular analyte have most often been considered ideal for LDPI-MS as they minimize the excess energy available for parent ion dissociation.<sup>9,10</sup> Different photon energies for SPI can readily be accessed at a VUV synchrotron light source.<sup>7,8,11,12</sup>

Another issue that arises in MS imaging is the difficulty of establishing analysis protocols on complex, heterogeneous biological samples. This difficulty has led to the use of organic multilayer models to evaluate the suitability of SIMS protocols for analysis of intact biological samples. SIMS studies of organic multilayer models have included Langmuir-Blodgett films of barium arachidate,<sup>13</sup> dipalmitoyl-phosphatidylcholine-sucrose multilayers<sup>14</sup> and peptide doped trehalose thin films.<sup>3</sup>

A polyelectrolyte multilayer (PEM) model was applied here that is particularly well-suited to evaluate MS imaging protocols for bacterial biofilms. This PEM was composed of alginate and chitosan, two high molecular weight biopolymers which simulate the extracellular polysaccharides of biofilms. These PEMs were prepared by electrostatic layer by layer assembly of these two oppositely charged polysaccharides.<sup>15</sup> This model also allowed introduction of small molecular analytes into the PEM, simulating the presence of metabolites, signaling molecules, and other species present within actual biofilms. Here, the small molecular analyte was 3,5-dibromotyrosine ( $\text{Br}_2\text{Y}$ ), which was electrostatically adsorbed to every alternating alginate layer of the PEM. The presence of bromine and the unique isotopic pattern of  $\text{Br}_2\text{Y}$  facilitated identification by MS.

This study examined LDPI-MS of neat  $\text{Br}_2\text{Y}$  films, neat PEMs, and PEMs with adsorbed  $\text{Br}_2\text{Y}$  ( $\text{Br}_2\text{Y}$ -PEMs). 25 keV  $\text{Bi}_3^+$  SIMS was also performed on these samples, given the several prior studies that used SIMS to study biofilms.<sup>2-5</sup> MS analysis was performed using a commercial SIMS instrument additionally configured for LDPI-MS by coupling to a desorption laser and a tunable VUV synchrotron beamline.<sup>7,8,16</sup> Samples were also analyzed with a home built LDPI-MS that utilized a 7.87 eV molecular fluorine laser for postionization.<sup>6</sup> Ionization energies (IEs) of  $\text{Br}_2\text{Y}$  were determined experimentally and compared to IEs from electronic structure calculations. The results are discussed in terms of SPI mechanisms and desorption of  $\text{Br}_2\text{Y}$ , both from neat films and PEMs.

## II. EXPERIMENTAL DETAILS

### A. Preparation and Verification of Br<sub>2</sub>Y films, PEMs, and Br<sub>2</sub>Y-PEMs

Br<sub>2</sub>Y films were prepared from solutions in (1:1 v:v) acetonitrile:water that were dried on gold-coated silicon substrates.

PEMs were prepared on gold-coated substrates as described previously.<sup>15,17</sup> PEMs were verified by attenuated total reflection Fourier transform infrared spectroscopy. Elemental content of the PEMs was determined by monochromatic X-ray photoelectron spectroscopy using instrumentation and procedures previously described.<sup>18</sup> Details of the preparation and verification of the PEMs are given in Supporting Information.

20 mg/ml  $\alpha$ -cyano-4-hydroxycinnamic acid (CHCA) matrix solutions were prepared in (7:3 v:v) acetonitrile:trifluoroacetic acid (0.1% v:v). These matrix solution were then sprayed onto a subset of the PEMs to facilitate desorption during 7.87 eV LDPI-MS.

### B. 8 – 12.5 eV Synchrotron LDPI-MS and SIMS

Synchrotron LDPI-MS and SIMS were recorded using a commercial SIMS instrument (TOF.SIMS 5, ION-TOF Inc., Munster, Germany) using 25 keV Bi<sub>3</sub><sup>+</sup> primary ions.<sup>8</sup> The SIMS instrument was modified for LDPI-MS by the addition of a 349 nm pulsed desorption laser (Explorer, Newport) operating at 2500 Hz with a spot size of ~30  $\mu$ m diameter and typical laser desorption peak power density of 1 to 10 MW/cm<sup>2</sup>. The laser desorbed neutral molecules were photoionized by 8.0 to 12.5 eV tunable VUV synchrotron radiation from the Chemical Dynamics Beamline at the Advanced Light Source (Lawrence Berkeley National Laboratory, Berkeley, CA)<sup>16</sup> 143,000 laser shots on a single spot were used for each displayed mass spectrum. This instrument was also used to record photoionization efficiency curves of gas phase Br<sub>2</sub>Y molecules. See Supporting Information for further details. The experimental mass resolution of this instrument for the parent ion from Br<sub>2</sub>Y films was 980 and 1100 for LDPI-MS and negative ion SIMS, respectively.

### C. 7.87 eV Laser LDPI-MS

7.87 eV laser LDPI-MS was collected using a custom built instrument at the University of Illinois at Chicago which is equipped with a 157.6 nm pulsed laser (7.87 eV) for photoionization and was described in detail previously.<sup>6</sup> This LDPI-MS has a 349 nm Nd:YLF desorption laser operating at 100 Hz, with a spot size of ~20  $\mu$ m diameter and typical desorption laser peak power density ranging from 30 to 70 MW/cm<sup>2</sup>. The sample was rastered at 100  $\mu$ m/s with respect to the laser, so each 20  $\mu$ m sample spot was sampled by ~20 desorption laser shots and a total of 50 – 100 laser shots were sufficient to obtain spectra with optimal signal to noise. See Supporting Information for further details. The experimental mass resolution of this instrument for the parent ion from Br<sub>2</sub>Y films was 420.

### D. Electronic Structure Calculations

Calculations were performed using density functional theory with a commercial quantum chemistry software package (Gaussian 03, Pittsburgh, PA).<sup>19</sup> Vertical ionization energies (IEs) were calculated for Br<sub>2</sub>Y, [Br<sub>2</sub>Y]<sub>2</sub>, [Br<sub>2</sub>Y][H<sub>2</sub>O] and [Br<sub>2</sub>Y][H<sub>2</sub>O]<sub>3</sub> (see Supporting Information for geometries and other details). The [Br<sub>2</sub>Y][H<sub>2</sub>O]<sub>3</sub> cluster was chosen as an intermediate species representative between what is expected to be highly abundant [Br<sub>2</sub>Y][H<sub>2</sub>O] and the much larger clusters thought to form in MALDI.<sup>20,21</sup>

### III. RESULTS AND DISCUSSION

#### A. Single Photon Ionization of Evaporated and Laser Desorbed Br<sub>2</sub>Y Films

The first experiments were designed to evaluate VUV SPI of Br<sub>2</sub>Y. The photoionization efficiency curve of evaporated Br<sub>2</sub>Y (see Supporting Information) was recorded by monitoring the parent ion at  $m/z$  337 while sweeping the VUV photon energy from the synchrotron. The experimental IE of Br<sub>2</sub>Y of  $8.3 \pm 0.1$  eV was determined from the extrapolation of the photoionization efficiency curve using the drawn lines and agreed well with the 8.3 eV IE determined by electronic structure calculations.

Next, Br<sub>2</sub>Y films on gold-coated substrates were laser desorbed and the resultant gaseous neutrals photoionized by VUV radiation and detected by time-of-flight MS. Figure 1 displays the LDPI-MS of Br<sub>2</sub>Y films recorded using both 7.87 eV laser and 8.0 eV synchrotron photoionization. Both display characteristic fragments and clusters of Br<sub>2</sub>Y. All Br-containing peaks are referred to below by their lowest mass isotopes (i.e., those composed of <sup>12</sup>C, <sup>79</sup>Br, and <sup>1</sup>H) and were verified by the unique 1:0.97 isotopic pattern for <sup>79</sup>Br:<sup>81</sup>Br (see below).

Control experiments showed no significant ion signal from Br<sub>2</sub>Y films except in the presence of both VUV radiation and the desorption laser (LD). This fact was demonstrated by the data in Figure 1 labeled “VUV only” and “LD only”, neither of which display any significant ion signal. Thus, few volatile species were detected by SPI at room temperature in the absence of laser desorption and little direct ionization occurred in the sole presence of the desorption laser.

The [Br<sub>2</sub>Y]<sup>+</sup> parent ion at  $m/z$  336.9 along with various low mass fragments of Br<sub>2</sub>Y appear in both the 7.87 eV laser and 8.0 eV synchrotron LDPI-MS in Figure 1. Figure 2 identifies each of these fragments by a Roman numeral and illustrates the proposed fragment structures.  $M/z$  302.9 (I) was attributed to the parent ion after loss of H<sub>2</sub>O<sub>2</sub>.  $M/z$  291.9 (II) was attributed to loss of COOH via cleavage of the  $\alpha$  C-C bond.  $M/z$  264.0 (III) was attributed to loss of NHCHCOOH via cleavage of the  $\beta$  C-C bond. These observations were consistent with prior VUV SPI studies that found amino acids predominantly undergo cleavage via the C-C bonds that are  $\alpha$  and  $\beta$  to the terminal carboxyl group.<sup>22–25</sup>  $M/z$  213.0 (IV) and  $m/z$  185.1 (V) underwent similar cleavages with the additional loss of Br (losses of BrCOOH and BrNHCHCOOH, respectively). The charge resided on the aromatic group for most of these fragment ions due to charge stabilization via delocalization.<sup>24</sup> However, some fraction of  $\beta$  C-C bond cleavage led to the charge residing on the carboxyl group and produced the  $m/z$  74.0 (VI) ion.

Some differences were observed between LDPI-MS using 7.87 eV laser and 8.0 eV synchrotron photoionization. The relative abundances of fragment ions differed with photoionization source and desorption conditions.  $M/z$  291.9 (II) appeared as the most intense peak by 7.87 eV laser photoionization while  $m/z$  264.0 (III) was the most intense peak by 8.0 eV synchrotron photoionization. However, the most significant difference was the sole appearance of Br<sup>+</sup> in the 8.0 eV synchrotron photoionization, as discussed further below.

Certain higher mass ions attributed to clusters of Br<sub>2</sub>Y were also observed at both 7.87 eV laser and 8.0 eV synchrotron photoionization energies, as shown in Figure 3. The peak envelope in Figure 3(a) at  $m/z$  561.8, 563.8, 565.8, and 567.8 with peak intensity ratios 1:3:3:1 matched with  $m/z$  and isotopic distribution for [Br<sub>3</sub>Y<sub>2</sub>-NH<sub>2</sub>H<sub>2</sub>O]H<sup>+</sup>, the dimer of Br<sub>2</sub>Y after loss of Br, NH<sub>2</sub>, and H<sub>2</sub>O. The other cluster at  $m/z$  482.9 was assigned as [Br<sub>2</sub>Y<sub>2</sub>-

$\text{NH}_2\text{H}_2\text{O}]\text{H}^+$ . These clusters were detected by both 7.87 eV laser and 8.0 eV synchrotron photoionization.

The appearance of the aforementioned ions in Figure 3 confirmed cluster formation during laser desorption from pure films of  $\text{Br}_2\text{Y}$ . Pure analyte and analyte/solvent cluster formation also explained the appearance of ion signal for the parent ion and fragments thereof (Figures 1a and 2), despite the fact that the 7.87 photon energy was lower than the  $\sim 8.3$  eV experimental IEs of  $\text{Br}_2\text{Y}$ . Electronic structure calculations found IEs of 7.8 eV for  $[\text{Br}_2\text{Y}]_2$ , 8.1 eV for  $[\text{Br}_2\text{Y}][\text{H}_2\text{O}]$  and 7.9 eV for  $[\text{Br}_2\text{Y}][\text{H}_2\text{O}]_3$ . These calculated IEs indicate that clustering between  $\text{Br}_2\text{Y}$  monomers or with water lowered their IEs below that of the monomer. Thus, the lower IEs of pure  $\text{Br}_2\text{Y}$  clusters and/or  $[\text{Br}_2\text{Y}]_m[\text{H}_2\text{O}]_{n>1}$  and their dissociation following photoionization enabled the detection of  $\text{Br}_2\text{Y}$  by 7.87 eV laser LDPI-MS, leading to essentially all of the ion signal observed in both Figures 1a and 3a.

Molecular dynamics simulations and experimental probes of the evolution of a desorption plume in the MALDI process showed that pulsed laser irradiation results in the ejection of a mixture of individual molecules, clusters, and microdroplets.<sup>20,21</sup> Previous studies also showed that IEs of clusters of pure analyte or analyte-solvent are substantially lower than their corresponding monomers. For example, clusters of proline and 2,5-dihydroxybenzoic acid displayed lower IEs than the free matrix or proline<sup>26</sup> as did cytosine dimers compared to monomers<sup>27</sup> and water clusters compared to isolated water molecules.<sup>28,29</sup> All of this prior work supports the cluster desorption/photoionization mechanism proposed here.

Another aspect of the clusters that  $\text{Br}_2\text{Y}$  forms with itself and/or water was that many, if not all, were protonated. Prior SPI of formic acid and water clusters found that protonated species dominated.<sup>28,30</sup> The two cluster species detected by both laser and synchrotron VUV SPI,  $[\text{Br}_2\text{Y}_2\text{-NH}_2\text{H}_2\text{O}]\text{H}^+$  and  $[\text{Br}_3\text{Y}_2\text{-NH}_2\text{H}_2\text{O}]\text{H}^+$ , were both protonated. Thus, all higher mass clusters observed solely in laser VUV SPI were also assigned as protonated, although their signal to noise ratios were insufficient to assign  $m/z$  values with  $<1$   $m/z$  accuracy.

The 7.87 laser LDPI-MS showed a  $\sim 0.05$  ratio of clusters to fragments, indicating a dominance of fragments in the spectra. The low excess energy available from threshold single photon ionization at 7.87 eV of clusters was insufficient to lead to such extensive cluster fragmentation. This is supported by the 9.45 eV SPI-MS of evaporated  $\text{Br}_2\text{Y}$ , which showed little fragmentation (see Supporting Information). However, cluster fragmentation would have been aided by the additional internal energy imparted by laser desorption. Furthermore, single photon ionization of clusters could have led to structural rearrangement and proton transfer to form some of the fragment ions depicted in Figure 2. Nevertheless, the details of cluster fragmentation remain unresolved: further experiments and calculations are needed to validate ion structures and fragmentation mechanisms.

The low photon energy and narrow bandwidth of the 7.87 eV laser support the ionization mechanism via lowered cluster IEs. However, the case with the 8.0 eV synchrotron LDPI-MS of the  $\text{Br}_2\text{Y}$  films in Figures 1b and 3b is less clear. The slightly higher 8.0 eV photon energy and the 0.2 eV bandwidth of the synchrotron radiation<sup>16</sup> left open the possibility of some threshold single photon ionization of  $\text{Br}_2\text{Y}$  and  $[\text{Br}_2\text{Y}][\text{H}_2\text{O}]$ . Furthermore, some signal may have resulted from a minor amount of photoelectron ionization<sup>31</sup> or higher VUV harmonics leaking through the gas filter in the synchrotron beamline causing photoionization, as discussed previously.<sup>32</sup> However, the similarity of the fragments and clusters for both 7.87 eV laser and 8.0 eV synchrotron radiation and the similar cluster to fragment ratios (except as noted below) argued for a common ionization mechanism.

Nevertheless, there were several significant differences between 7.87 eV laser and 8.0 eV synchrotron radiation of  $\text{Br}_2\text{Y}$  films. The high mass  $\text{Br}_2\text{Y}$  spectra showed a higher mass



distribution of clusters for 7.87 eV laser photoionization. These higher mass clusters included the intact protonated dimer,  $[\text{Br}_4\text{Y}_2]\text{H}^+$ , the trimer after a single Br loss,  $[\text{Br}_5\text{Y}_3]\text{H}^+$ , and fragments thereof. The source of this difference was not determined, but likely resulted from differences in either desorption/ionization conditions and/or TOF collection/transmission efficiencies between the two instruments.

Another significant difference between the  $\text{Br}_2\text{Y}$  spectra from the two photoionization sources was the observation of a peak at  $m/z$  78.9 due to  $\text{Br}^+$  only for 8.0 eV synchrotron photoionization (Figure 1). This result led to experiments in which the tunability of synchrotron radiation was exploited to record the LDPI-MS of  $\text{Br}_2\text{Y}$  films at photon energies above 8.0 eV (see Supporting Information). Increasing the photon energy from 8.0 to 12.5 eV showed only modest changes in the fragmentation pattern for  $\text{Br}_2\text{Y}$ , which remained different from those of 11.5 eV SPI-MS of evaporated  $\text{Br}_2\text{Y}$ . However, the signal intensity for all fragments did increase with photon energy, presumably due to a corresponding increase in the photoionization cross sections of the desorbed clusters.

Intense signals for both  $\text{Br}^+$  at  $m/z$  78.9 and  $\text{Br}_2^+$  at  $m/z$  157.8 were observed at photon energies in excess of their ionization energies of 11.81 and 10.52 eV, respectively. The 349 nm wavelength of the desorption laser is sufficient to induce photodissociation of various organic bromides via the C-Br bond whose  $\sim 3$  eV bond energy is readily cleaved to form bromine and carbon radicals.<sup>33,34</sup>  $\text{Br}_2$  could have formed from surface adsorbed Br that recombined during laser induced thermal desorption, analogous to the formation of  $\text{O}_2$  by laser induced thermal desorption of atomic oxygen on metal surfaces.<sup>35</sup> Examination of the time evolution of the Br and  $\text{Br}_2$  signal (data of spectra versus laser shot recorded from a single sample spot not shown) indicated a relative increase in their signal over time compared to the  $\text{Br}_2\text{Y}$  fragment ions and clusters. This time evolution supported a  $\text{Br}_2\text{Y}$  degradation mechanism for the formation of Br and  $\text{Br}_2$ . This degradation might also explain some of the differences in fragment ratios between laser and synchrotron photoionization.

Neither Br nor  $\text{Br}_2$  was detected by 7.87 eV laser photoionization (see Figure 1).  $\text{Br}_2^+$  was only observed by synchrotron photoionization with photon energies at and above the 10.52 eV  $\text{Br}_2$  IE. However,  $\text{Br}^+$  was observed with 8.0 eV synchrotron radiation and at other photon energies below the 11.81 eV ionization energy of the Br atom: it may have formed by the same low photon energy mechanisms discussed above for the experiments using synchrotron radiation.

## B. LDPI-MS of Polyelectrolyte Multilayers: Neat PEMs and $\text{Br}_2\text{Y}$ -PEMs

The above results established the ability of VUV SPI to detect  $\text{Br}_2\text{Y}$  as neat films, so the next step was to examine the conditions required to detect  $\text{Br}_2\text{Y}$  adsorbed into PEMs. These  $\text{Br}_2\text{Y}$ -PEMs and also neat PEMs (without  $\text{Br}_2\text{Y}$ ) were analyzed by LDPI-MS using both 7.87 eV laser and 11.5 eV synchrotron photoionization, with the higher photon energy chosen at the synchrotron for its large expected photoionization cross sections.

Figure 4 shows 7.87 eV laser LDPI-MS of  $\text{Br}_2\text{Y}$ -PEMs, analyzed with and without CHCA matrix added to the fully prepared multilayer prior to MS analysis. The CHCA-treated sample allowed matrix-assisted laser desorption of neutral species, which produced  $m/z$  264.0 (III) and  $m/z$  291.9 (II) ions upon single photon ionization. These two ions were previously observed as the most intense ions formed from the neat  $\text{Br}_2\text{Y}$  films (see Figures 1 and 2). The ion observed at  $m/z$  189.0 in Figure 4 was attributed to the CHCA parent ion and  $m/z$  210 was attributed to the  $[\text{CHCA}\cdot\text{Na}]^+$  complex while  $m/z$  145.6 and several lower  $m/z$  peaks were assigned as CHCA fragments. All CHCA-only peaks are marked with asterisks in Figure 4.

The spectrum of the Br<sub>2</sub>Y-PEM without matrix shows no Br<sub>2</sub>Y-attributed peaks. Rather, it only displays peaks below  $m/z$  150, none of which were assignable to any characteristic fragment of Br<sub>2</sub>Y. The various controls supported these results. The spectrum of PEM with CHCA displays only matrix-associated peaks. LD only of both Br<sub>2</sub>Y-PEM and neat PEM without the VUV laser showed no signal either with or without added CHCA matrix, indicating that direct ionization did not occur at these desorption laser peak power densities, which were similar to those used to analyze the pure Br<sub>2</sub>Y films.

The inability to detect any Br containing species with 7.87 eV laser photoionization when no matrix was added raises the question of how much Br<sub>2</sub>Y was actually adsorbed into the Br<sub>2</sub>Y-PEMs. X-ray photoelectron spectra were recorded on equivalent Br<sub>2</sub>Y-PEM samples and indicated a 0.7% bromine content, compared to a calculated value of 13% for a pure Br<sub>2</sub>Y film. Thus, the Br<sub>2</sub>Y-PEMs had ~5% of the total Br<sub>2</sub>Y of pure films, yet no Br-containing species could be observed in the absence of matrix. This ~5% Br<sub>2</sub>Y concentration was apparently insufficient to allow the cluster formation needed for 7.87 eV SPI under these desorption conditions. By contrast, the matrix facilitated desorption of pure Br<sub>2</sub>Y clusters or mixed Br<sub>2</sub>Y/CHCA/water clusters, all of which were expected to display ionization energies below the 7.87 eV photon energy (see above). The applied matrix on the PEM probably also extracted some of the Br<sub>2</sub>Y into a surface layer where it co-crystallized with the matrix and permitted matrix assisted laser desorption, as is thought to occur in standard MALDI-MS.<sup>21</sup>

Next, the ionizing photon energy was raised in an attempt to detect adsorbed Br<sub>2</sub>Y in the Br<sub>2</sub>Y-PEM without the addition of matrix. Br<sub>2</sub>Y was detected by 11.5 eV synchrotron LDPI-MS, as manifested in the  $m/z$  185.1 (V) and  $m/z$  264.0 (III) peaks from the Br<sub>2</sub>Y-PEM, as shown in Figure 5. Experiments were performed in which the desorption laser peak power density was increased, but it neither enhanced the useful III/V fragment signal nor brought out any other peaks that were clearly characteristic of Br<sub>2</sub>Y (data not shown). Rather, higher desorption laser peak power densities only led to more PEM degradation as characterized by pyrolysis peaks appearing at almost every integer  $m/z$  value up to  $\sim m/z$  450.

### C. SIMS of Br<sub>2</sub>Y Films, Neat PEMs, and Br<sub>2</sub>Y-PEMs

Films of Br<sub>2</sub>Y, neat PEMs, and Br<sub>2</sub>Y-PEMs were also analyzed by 25 keV Bi<sub>3</sub><sup>+</sup> SIMS. While the positive ion spectra were relatively uninteresting (see Supporting Information), the negative ion SIMS of the Br<sub>2</sub>Y films and Br<sub>2</sub>Y-PEMs in Figure 6 display significant useful signal.

The negative ion SIMS of the Br<sub>2</sub>Y films displayed the [Br<sub>2</sub>Y]<sup>-</sup> parent ion at  $m/z$  336.9, and strong Br<sup>-</sup> and Br<sub>2</sub><sup>-</sup> peaks. Several other Br<sub>2</sub>Y-related peaks also appeared including one at  $m/z$  262.9 that was similar to the structure III (see Figure 2) minus a proton, denoted as [III-H]<sup>-</sup> in Figure 6. Other Br<sub>2</sub>Y characteristic ion appeared at  $m/z$  249.9 that was attributed to the III structure without the CH<sub>2</sub> group and denoted as [III-CH<sub>2</sub>]<sup>-</sup>. The clusters of peaks near  $m/z$  290 were attributed to an overlap of the II ion and the II ion minus a proton, [II-H]<sup>-</sup>. The peak at  $m/z$  275.9 was attributed to [II-NH<sub>2</sub>]<sup>-</sup>. Thus, SIMS observed several fragments not seen in LDPI-MS. No ions were observed in the negative ion SIMS with structures related to the I, IV, V, or VI ions observed in LDPI-MS. Finally, the peak at  $m/z$  417.8 also appeared related to Br<sub>2</sub>Y and was tentatively assigned to [Br<sub>2</sub>Y][HBr]<sup>-</sup>, although at least one other assignment related to fragments of dimerized Br<sub>2</sub>Y was also feasible. The Br<sub>2</sub>Y-PEMs also displayed the [Br<sub>2</sub>Y]<sup>-</sup> parent ion and Br<sup>-</sup>, but did not display the structurally intact (II/III related) fragments of Br<sub>2</sub>Y that were observed for the negative ion SIMS of the neat Br<sub>2</sub>Y films. However, other Br-containing ions were observed including  $m/z$  157.8 corresponding to Br<sub>2</sub><sup>-</sup>,  $m/z$  180.8 corresponding to [Br<sub>2</sub>Na]<sup>-</sup> and  $m/z$  283.5 corresponding to [Br<sub>3</sub>Na<sub>2</sub>]<sup>-</sup>. Br<sub>2</sub>Y-PEM also showed a peak at  $m/z$  359.4 assigned to [Br<sub>2</sub>Y]

$[\text{Na}]^-$  and several other peaks up to  $m/z$  550 with characteristic bromine isotopic patterns indicative of other  $[\text{Br}_2\text{Y}][\text{Na}_x\text{Br}_y]^-$  or  $[\text{Na}_x\text{Br}_y]^-$  structures. Some of the most prominent ions in the negative ion SIMS of the  $\text{Br}_2\text{Y}$ -PEMs showed high sensitivity to Br, but these atomic  $[\text{Na}_x\text{Br}_y]^-$  clusters contained little information on the analyte's chemical structure. That these various negative ion adducts containing Na appeared only in the  $\text{Br}_2\text{Y}$ -PEM spectra was attributed to the presence of excess sodium from the sodium alginate used in their preparation and/or a unique desorption event facilitated by the PEM (or the complexation of  $\text{Br}_2\text{Y}$  therein). The neat PEMs showed none of the above mentioned peaks associated with  $\text{Br}_2\text{Y}$  (see Figure 6).

#### IV. CONCLUSIONS

These results demonstrated several points of significance to the application of VUV SPI to MS imaging. It has usually been considered necessary for the VUV photon energy to exceed a molecular analyte's ionization energy to allow SPI.<sup>10</sup> However, the lower ionization energy of pure analyte, anal/solvent, or analyte/matrix clusters that form during laser desorption can permit SPI at lower photon energies.<sup>26,27,36</sup> The practical implication of this observation is that the fluorine excimer laser might be much more widely useful for VUV postionization in MS imaging, as it can detect some species with ionization energies above its 7.87 eV photon energy when they cluster.

Cluster formation does require a relatively high density of gaseous species that could be laser desorbed only from pure films or polyelectrolyte multilayers pretreated with matrix. Thus, even the relatively high (~5%) fraction of adsorbed  $\text{Br}_2\text{Y}$  in the polyelectrolyte multilayers was insufficient to produce clusters upon laser desorption unless CHCA matrix was added prior to analysis. The application of matrix was also thought to facilitate extraction of adsorbed  $\text{Br}_2\text{Y}$  from within the multilayer while also enhancing the explosive desorption known to occur in MALDI.<sup>20,21</sup> Desorption was enhanced by matrix even though desorption laser peak power density was kept low enough to minimize direct ion formation via proton transfer. Nevertheless,  $\text{Br}_2\text{Y}$  was detectable from multilayers without added matrix when higher photon energies were employed for SPI.

The positive ion spectra from  $\text{Bi}_3^+$  SIMS produced few useful results for these samples, showing mostly monomers of the polysaccharides (see Supporting Information).<sup>37,38</sup> However, the negative ion spectra were analytically quite useful. Like many organohalides,  $\text{Br}_2\text{Y}$  has a high electron affinity, which is expected to enhance negative ion formation.<sup>39</sup> However, most non-halogenated analytes have low electron affinities and may not produce as useful a negative signal. Furthermore, there was a strong dependence of the analyte's condensed phase environment upon the negative SIMS, with the neat films displaying major differences from the multilayer spectra.

Finally, a few observations can be made regarding the comparison of LDPI-MS with SIMS. SIMS permits much higher spatial resolution for MS imaging of ~100 nm, compared with a spatial resolution of ~20  $\mu\text{m}$  for LDPI-MS, similar to that observed for MALDI-MS.<sup>40</sup> Both methods formed significant parent ions from the pure  $\text{Br}_2\text{Y}$  films, albeit via different ionization pathways. However, the SPI event in LDPI-MS formed additional fragment and cluster ion species not observed in SIMS. The difference in spectra from the two methods was even greater for the  $\text{Br}_2\text{Y}$ -PEMs, mostly due to differences in the extent and type of fragmentation and clustering. It can be concluded that LDPI-MS and SIMS will generally provide complementary chemical information due to their different ionization mechanisms. Furthermore, the ability to tune the ionization event by selection of photon energy in SPI adds an added dimension of selectivity to LDPI-MS that is not directly available in SIMS. This work has refrained from comparisons of sensitivity between LDPI-MS and SIMS, as



the former was performed using novel experimental configurations that are the subject of ongoing improvements.

## Supplementary Material

Refer to Web version on PubMed Central for supplementary material.

## Acknowledgments

The authors acknowledge the assistance of Jerry F. Moore and Oleg Kostko with various aspects of the data collection and analysis. This work is supported by the National Institute of Biomedical Imaging and Bioengineering via grant EB006532. The contents of this manuscript are solely the responsibility of the authors and do not necessarily represent the official views of the National Institute of Biomedical Imaging and Bioengineering or the National Institutes of Health. MA, LT, JZ and the Advanced Light Source are supported by the Director, Office of Energy Research, Office of Basic Energy Sciences, Chemical Sciences Division of the U.S. Department of Energy under contract No. DE-AC02-05CH11231.

## References

1. Otto M. *Nat Rev Microbiol.* 2009; 7:555. [PubMed: 19609257]
2. Tyler BJ, Rangarajan S, Möller J, Beumer A, Arlinghaus HF. *Appl Surf Sci.* 2006; 252:6712.
3. Wucher A, Cheng J, Winograd N. *Anal Chem.* 2007; 79:5529. [PubMed: 17583913]
4. Fletcher JS. *Analyst.* 2009; 134:2204. [PubMed: 19838405]
5. Esquenazi E, Yang YL, Watrous J, Gerwick WH, Dorrestein PC. *Nat Prod Rep.* 2009; 26:1521. [PubMed: 19936384]
6. Akhmetov A, Moore JF, Gasper GL, Koin PJ, Hanley L. *J Mass Spectrom.* 2010; 45:137. [PubMed: 20146224]
7. Gasper GL, Takahashi LK, Zhou J, Ahmed M, Moore JF, Hanley L. *Anal Chem.* 2010; 82:7472. [PubMed: 20712373]
8. Takahashi LK, Zhou J, Wilson KR, Leone SR, Ahmed M. *J Phys Chem A.* 2009; 113:4035. [PubMed: 19371112]
9. Zhou J, Takahashi LK, Wilson KR, Leone SR, Ahmed M. *Anal Chem.* 2010; 82:3905. [PubMed: 20353160]
10. Hanley L, Zimmermann R. *Anal Chem.* 2009; 81:4174. [PubMed: 19476385]
11. Li Y, Qi F. *Acc Chem Res.* 2009; 43:68. [PubMed: 19705821]
12. Gasper, GL.; Takahashi, LK.; Zhou, J.; Ahmed, M.; Moore, JF.; Hanley, L. *Nucl Instr Meth Phys Res A.* 2011. in press. <http://dx.doi.org/10.1016/j.nima.2010.12.024>
13. Sostarecz AG, Sun S, Szakal C, Wucher A, Winograd N. *Appl Surf Sci.* 2004; 231/232:179.
14. Kozole J, Szakal C, Kurczy M, Winograd N. *Appl Surf Sci.* 2006; 252:6789.
15. Deng T, Wang H, Li J, Hu S, Shen G, Yu R. *Sens Actuat B.* 2004; 99:123.
16. Heimann PA, Koike M, Hsu CW, Blank D, Yang XM, Suits AG, Lee YT, Evans M, Ng CY, Flaim C, Padmore HA. *Rev Sci Instrum.* 1997; 68:1945.
17. Maurstad G, Morch YA, Bausch AR, Stokke BT. *Carbohydr Polym.* 2008; 71:672.
18. Crot CA, Wu C, Schlossman ML, Trainor TP, Eng PJ, Hanley L. *Lang.* 2005; 21:7899.
19. Frisch, MJ.; Trucks, GW.; Schlegel, HB.; Scuseria, GE.; Robb, MA.; Cheeseman, JR.; Montgomery, JAJ.; Vreven, T.; Kudin, KN.; Burant, JC.; Millam, JM.; Iyengar, SS.; Tomasi, J.; Barone, V.; Mennucci, B.; Cossi, M.; Scalmani, G.; Rega, N.; Petersson, GA.; Nakatsuji, H.; Hada, M.; Ehara, M.; Toyota, K.; Fukuda, R.; Hasegawa, J.; Ishida, M.; Nakajima, T.; Honda, Y.; Kitao, O.; Nakai, H.; Klene, M.; Li, X.; Knox, JE.; Hratchian, HP.; Cross, JB.; Adamo, C.; Jaramillo, J.; Gomperts, R.; Stratmann, RE.; Yazyev, O.; Austin, AJ.; Cammi, R.; Pomelli, C.; Ochterski, JW.; Ayala, PY.; Morokuma, K.; Voth, GA.; Salvador, P.; Dannenberg, JJ.; Zakrzewski, VG.; Dapprich, S.; Daniels, AD.; Strain, MC.; Farkas, O.; Malick, DK.; Rabuck, AD.; Raghavachari, K.; Foresman, JB.; Ortiz, JV.; Cui, Q.; Baboul, AG.; Clifford, S.; Cioslowski, J.; Stefanov, BB.; Liu, G.; Liashenko, A.; Piskorz, P.; Komaromi, I.; Martin, RL.; Fox, DJ.; Keith,

- T.; Al-Laham, MA.; Peng, CY.; Nanayakkara, A.; Challacombe, M.; Gill, PMW.; Johnson, B.; Chen, W.; Wong, MW.; Gonzalez, C.; Pople, JA. Gaussian 03, Revision A.1. Gaussian, Inc; 2003.
20. Rohlving A, Leisner A, Hillenkamp F, Dreisewerd K. *J Phys Chem C*. 2009; 114:5367.
  21. Knochenmuss R, Zhigilei LV. *J Mass Spectrom*. 2010; 45:333. [PubMed: 20301182]
  22. Jochims HW, Schwell M, Chotin JL, Clemeno M, Dulieu F, Baumgärtel H, Leach S. *Chem Phys*. 2004; 298:279.
  23. Schwell M, Jochims HW, Baumgärtel H, Dulieu F, Leach S. *Planet Space Sci*. 2006; 54:1073.
  24. Edirisinghe PD, Moore JF, Calaway WF, Veryovkin IV, Pellin MJ, Hanley L. *Anal Chem*. 2006; 78:5876. [PubMed: 16906735]
  25. Zhang L, Pan Y, Guo H, Zhang T, Sheng L, Qi F, Lo PK, Lau KC. *J Phys Chem A*. 2009; 113:5838. [PubMed: 19400571]
  26. Kinsel GR, Knochenmuss R, Setz P, Land CM, Goh SK, Archibong EF, Hardesty JH, Marynick DS. *J Mass Spectrom*. 2002; 37:1131. [PubMed: 12447889]
  27. Kostko O, Bravaya K, Krylov A, Ahmed M. *Phys Chem Chem Phys*. 2010; 12:2860. [PubMed: 20449376]
  28. Belau L, Wilson KR, Leone SR, Ahmed M. *J Phys Chem A*. 2007; 111:10075. [PubMed: 17715907]
  29. Barth S, Oncak M, Ulrich V, Mucke M, Lischke T, Slavicek P, Hergenbahn U. *J Phys Chem A*. 2009; 113:13519. [PubMed: 19856943]
  30. Heinbuch S, Dong F, Rocca JJ, Bernstein ER. *J Chem Phys*. 2007; 126:244301. [PubMed: 17614543]
  31. Gamez G, Zhu L, Schmitz TA, Zenobi R. *Anal Chem*. 2008; 80:6791. [PubMed: 18665611]
  32. Suits AG, Heimann P, Yang X, Evans M, Hsu C-W, Lu K-t, Lee YT, Kung AH. *Rev Sci Instrum*. 1995; 66:4841.
  33. Scaiano JC, Barra M, Sinta R. *Chem Mater*. 1996; 8:161.
  34. Huang J, Xu D, Francisco JS, Jackson WM. *J Chem Phys*. 2003; 118:3083.
  35. Hanley L, Kornienko O, Ada ET, Fuoco E, Trevor JL. *J Mass Spectrom*. 1999; 34:705. [PubMed: 10407355]
  36. Marchi I, Rudaz S, Veuthey J. *Talanta*. 2009; 78:1–18. [PubMed: 19174196]
  37. Tam SK, Dusseault J, Polizu S, Menard M, Halle JP, Yahia LH. *Biomater*. 2005; 26:6950.
  38. Sjovald P, Lausmaa J, Johansson BL, Andersson M. *Anal Chem*. 2004; 76:1857. [PubMed: 15053644]
  39. Harrison, AG. *Chemical Ionization Mass Spectrometry*. CRC Press; Boca Raton: 1992.
  40. Chughtai K, Heeren RMA. *Chem Rev*. 2010; 110:3237. [PubMed: 20423155]

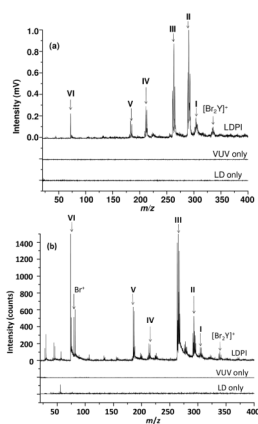


**Figure 1.** (a) 7.87 eV laser and (b) 8.0 eV synchrotron LDPI-MS of  $\text{Br}_2\text{Y}$  films: low mass range. The fragment ion structures associated with the Roman numeral labels are given in Figure 2.

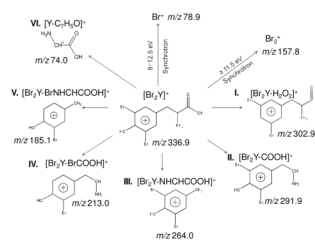


**Figure 2.** Schematic diagram of the fragmentation of  $\text{Br}_2\text{Y}$  by 7.87 eV laser and 8 - 12.5 eV synchrotron LDPI-MS, with Roman numerals identifying fragment ions.  $\text{Br}^+$  and  $\text{Br}_2^+$  were only observed by synchrotron photoionization at the noted photon energies.

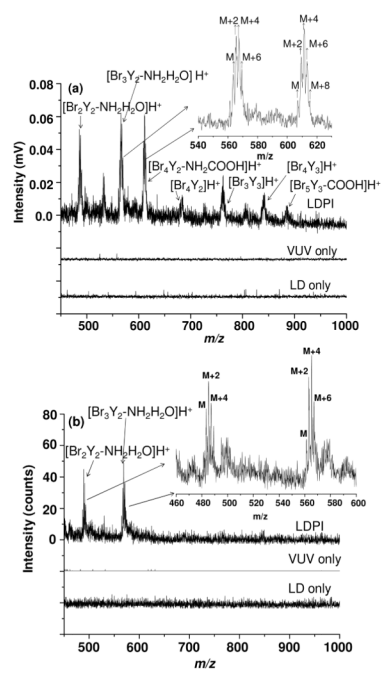


**Figure 3.**  
 (a) 7.87 eV laser and (b) 8.0 eV synchrotron LDPI-MS of  $\text{Br}_2\text{Y}$  films: high mass range.



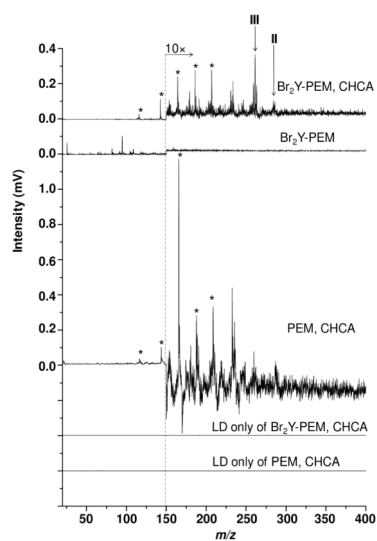


**Figure 4.** 7.87 eV laser LDPI-MS of Br<sub>2</sub>Y-PEM (top trace) with CHCA matrix; (second trace from top) without CHCA, but with Br<sub>2</sub>Y; and (third trace from top) with CHCA, but without Br<sub>2</sub>Y. The corresponding LD only of samples containing matrix are also shown. CHCA-only associated peaks marked with asterisks.

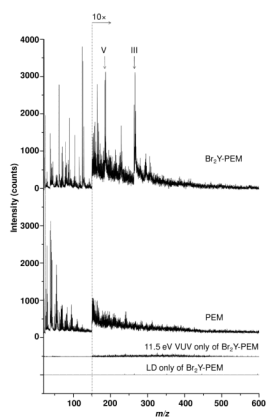


**Figure 5.** 11.5 eV synchrotron LDPI-MS of Br<sub>2</sub>Y-PEMs and neat PEMs. The 11.5 eV SPI-MS and LD only mass spectra for Br<sub>2</sub>Y-PEMs are also shown. No CHCA or other matrix was added.

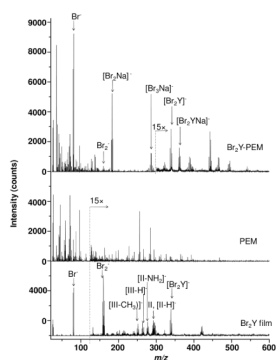


**Figure 6.** 25 keV  $\text{Bi}_3^+$  SIMS negative ion spectra of a  $\text{Br}_2\text{Y}$  film, neat PEM, and  $\text{Br}_2\text{Y}$ -PEM.